

Experimental Detection of Entanglement Polytopes via Local Filters

Yuanyuan Zhao,^{1,2} Markus Grassl,^{3,4} Bei Zeng,^{5,6} Guoyong Xiang,^{1,2,*}
Chao Zhang,^{1,2} Chuanfeng Li,^{1,2} and Guangcan Guo^{1,2}

¹Key Laboratory of Quantum Information, University of Science and Technology of China, CAS, Hefei, 230026, People's Republic of China

²Synergetic Innovation Center of Quantum Information and Quantum Physics,
University of Science and Technology of China, Hefei, Anhui 230026, People's Republic of China

³Institut für Optik, Information und Photonik, Universität Erlangen-Nürnberg, Erlangen, Germany

⁴Max-Planck-Institut für die Physik des Lichts, Erlangen, Germany

⁵Department of Mathematics & Statistics, University of Guelph, Guelph, Ontario, Canada

⁶Institute for Quantum Computing, University of Waterloo, Waterloo, Ontario, Canada

Entanglement polytopes result in finitely many types of entanglement that can be detected by only measuring single-particle spectra. With high probability, however, the local spectra lie in more than one polytope, hence providing no information about the entanglement type. To overcome this problem, we propose to additionally use local filters. We experimentally demonstrate the detection of entanglement polytopes in a four-qubit system. Using local filters we can distinguish the entanglement type of states with the same single particle spectra, but which belong to different polytopes.

PACS numbers: 03.65.Ud, 03.67.Mn, 71.10.Pm, 73.43.Nq

Entanglement among quantum systems is a kind of quantum correlation that is stronger than any possible classical correlation [1]. At the fundamental level, entanglement is the very mystery of quantum mechanics; and at the practical level, it can be used as a physical resource to perform computation and communication tasks that are impossible for classical systems. Essentially, entanglement comes from the tensor product structure of the Hilbert space of N systems—qubits in our case. An N -qubit quantum state $|\Psi_N\rangle$ is entangled if it can not be factored into products of quantum states of each of the qubits.

One central question regarding entanglement is that how $|\Psi_N\rangle$ may be entangled and how to detect that feature in practice. An obvious fact is that the parameters needed to specify $|\Psi_N\rangle$ grows exponentially with N . A natural idea to eliminate some of the free parameters is to take that two states $|\Psi_N\rangle$ and $|\Phi_N\rangle$ have similar entanglement features if they can be connected by some single-qubit operations, for instance, local unitary (LU) transformation [2–4] or stochastic local operation combined with classical communication (SLOCC) [5–7].

For $N = 2$, the Schmidt decomposition tells us that $|\Psi_2\rangle = \lambda_0|00\rangle + \lambda_1|11\rangle$ up to LU, with $\lambda_0 \geq \lambda_1$ and $\lambda_0^2 + \lambda_1^2 = 1$. Different $\lambda_0 \in [1/\sqrt{2}, 1]$ corresponds to different LU classes of entanglement, which are in fact infinitely many. Up to SLOCC, however, there is only one class of entangled states which contains the EPR pair with $\lambda_0 = 1/\sqrt{2}$. For $N = 3$, up to SLOCC, there are only two types of entanglement: the GHZ-type state and the W -type state [5]. These two types can be distinguished by a quantity called 3-tangle, which is however not a single-copy observable and hence cannot be directly measured in experiment [8] (that is, to get the value of 3-tangle, one either needs to measure jointly on multiple copies of the states, or needs a state tomography [9]).

For any $N > 3$, SLOCC no longer results in a finite number

of entanglement types [6, 7]. Despite the efforts of studying SLOCC classification of entanglement for $N > 3$ systems, the exponential growth of parameters with N for describing $|\Psi_N\rangle$ makes it hopeless to extract clear physical meanings of these classifications. It is highly desired to coarse-grain these classes such that we can grasp the key features of each entanglement type. The concept of entanglement polytopes provides an elegant idea to meet this need [10], where for each N there exists only finite number of types. More importantly, the polytopes are directly detectable in experiments via measuring only single-particle spectra of each qubit [10–12].

In this work, we experimentally demonstrate the detection of entanglement polytopes in a four-qubit system. Unfortunately, it turns out that different entanglement polytopes form a nested hierarchy [10–12], and they may have a large overlap. If the vector of local spectra of a state $|\Psi_N\rangle$ lies in an overlapping region, then we cannot uniquely identify the polytope that $|\Psi_N\rangle$ belongs to (see e.g. a recent experiment in which the states are chosen to be in non-overlapping regions [13]).

It turns out that for a randomly chosen three-qubit pure state $|\Psi_3\rangle$, the probability that the vector of local spectra of $|\Psi_3\rangle$ lies in the overlapping region of the W and GHZ polytopes is $\approx 94\%$. In general, for a randomly chosen state N -qubit state $|\Psi_N\rangle$, with high probability the vector of local spectra falls in some overlapping region of polytopes (we include a more detailed discussion of these probabilities in the Appendix). To overcome this difficulty, we use local filters (see, e.g. [14–18]) to effectively distinguish states with the same single particle spectra, but which belong to different polytopes.

Entanglement Polytopes – An N -qubit quantum state $|\Psi_N\rangle$ is said to be convertible to another N -qubit state $|\Phi_N\rangle$ via SLOCC if there exists a sequence of local operations and classical communication that converts the state $|\Psi_N\rangle$ to $|\Phi_N\rangle$ with nonzero probability. The states $|\Psi_N\rangle$ and $|\Phi_N\rangle$ are said

to be SLOCC equivalent if $|\Phi_N\rangle$ is convertible to $|\Phi_N\rangle$ and vice versa. It has been shown that $|\Psi_N\rangle$ is SLOCC equivalent to $|\Phi_N\rangle$ if and only if there exist invertible matrices M_i for $i = 1, 2, \dots, N$ such that

$$|\Psi_N\rangle = M_1 \otimes M_2 \otimes \dots \otimes M_N |\Phi_N\rangle. \quad (1)$$

This SLOCC equivalence relation partitions all N -qubit pure states into SLOCC equivalent classes, called the SLOCC orbits.

For an N -qubit state $|\Psi_N\rangle$, each of the single-particle reduced density matrices ρ_i for $i = 1, \dots, N$ has two eigenvalues $\lambda_i^\alpha, \lambda_i^\beta$ that are normalized, i.e. $\lambda_i^\alpha + \lambda_i^\beta = 1$. It suffices to consider the maximum eigenvalue of ρ_i , i.e. $\lambda_i^{\max} = \max(\lambda_i^\alpha, \lambda_i^\beta)$, with $\frac{1}{2} \leq \lambda_i^{\max} \leq 1$. The N -dimensional vector $\vec{\lambda} = (\lambda_1^{\max}, \lambda_2^{\max}, \dots, \lambda_N^{\max})$ then corresponds to a point in \mathbb{R}^N .

It has been shown that for the closure of an N -qubit SLOCC orbit $\bar{\mathcal{O}}$ of Ψ_N (i.e. some M_i in (1) possibly non-invertible), all the points $\vec{\lambda}$ of all $\bigotimes_{i=1}^N M_i |\Psi_N\rangle \in \bar{\mathcal{O}}$ form a polytope in \mathbb{R}^N , called the entanglement polytope of $\bar{\mathcal{O}}$. Moreover, for any finite N , there are only finitely many polytopes. This provides a natural classification of entanglement for N -qubit states, which ‘coarse-grains’ the infinitely many SLOCC orbits (for $N > 3$). Since the entanglement polytope for an SLOCC orbit is fully determined by the local spectra of the states in the orbit, this offers an appealing experimental approach for identifying the entanglement type for an N -qubit system, for which only measurements on single particles are required.

As a simple example, for $N = 3$, with only two kinds of SLOCC orbits (GHZ and W -type states), there are two polytopes in \mathbb{R}^3 . The polytope \mathcal{P}^{GHZ} corresponds to the GHZ-type states, with vertices $(1/2, 1/2, 1/2)$, $(1/2, 1/2, 1)$, $(1/2, 1, 1/2)$, $(1, 1/2, 1/2)$, $(1, 1, 1)$; and \mathcal{P}^W corresponds to the W -type states, with vertices $(1, 1, 1)$, $(1/2, 1/2, 1)$, $(1/2, 1, 1/2)$, $(1, 1/2, 1/2)$. Obviously, $\mathcal{P}^W \subset \mathcal{P}^{\text{GHZ}}$, which shows that entanglement polytopes for different SLOCC orbits may overlap.

In practice, for a state $|\Psi_N\rangle$, while a point $\vec{\lambda}$ may clearly distinguish its entanglement type, if $\vec{\lambda}$ is in an overlapping region of two polytopes, we fail to get information on which entanglement type the state belongs to. In the $N = 3$ case, for instance, this means that a point $\vec{\lambda} \in \mathcal{P}^W$ fails to distinguish the W -type entanglement from the GHZ-type entanglement. Unfortunately, for a randomly chosen pure state of three qubits, with $\approx 94\%$ probability the corresponding $\vec{\lambda}$ falls into \mathcal{P}^W .

Luckily, one can apply local filter operations $\bigotimes_{i=1}^N M_i$ to the system to ‘move around’ $\vec{\lambda}$, with the hope that $\vec{\lambda}$ ends up in a non-overlapping area of polytopes. As demonstrated in the three-qubit case, this step becomes crucial in practice when using the polytope method for detecting entanglement types, as the probability of overlapping is high.

Four-qubit Polytopes – Our experiments demonstrate the detection of entanglement types of four-qubit states. In this case, there are infinitely many SLOCC orbits. The full poly-

tope, containing $\vec{\lambda}$ for any four-qubit state, denoted by $\mathcal{P}^{\text{full}}$, is spanned by the vertices

$$\begin{aligned} &(\frac{1}{2}, \frac{1}{2}, \frac{1}{2}, \frac{1}{2}), (1, 1, 1, 1), \\ &(1, 1, \frac{1}{2}, \frac{1}{2}), (1, \frac{1}{2}, 1, \frac{1}{2}), (1, \frac{1}{2}, \frac{1}{2}, 1), \\ &(\frac{1}{2}, 1, 1, \frac{1}{2}), (\frac{1}{2}, 1, \frac{1}{2}, 1), (\frac{1}{2}, \frac{1}{2}, 1, 1), \\ &(\frac{1}{2}, \frac{1}{2}, \frac{1}{2}, 1), (\frac{1}{2}, 1, \frac{1}{2}, \frac{1}{2}), (\frac{1}{2}, \frac{1}{2}, 1, \frac{1}{2}), (\frac{1}{2}, \frac{1}{2}, \frac{1}{2}, 1). \end{aligned}$$

Up to permutation of the qubits, there are 6 other polytopes inside $\mathcal{P}^{\text{full}}$, which may also be mutually overlapping. Similar as in the $N = 3$ case, for a randomly chosen four-qubit state, the chance that $\vec{\lambda}$ lies in an overlapping region is high (for details, see the Appendix). Therefore, we have to apply local operations to ‘move around’ $\vec{\lambda}$. The proposed experiment is given by the diagram in Fig. 1.

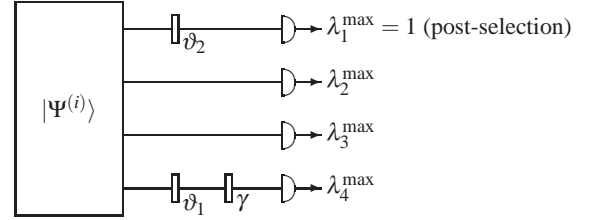


FIG. 1: Circuit diagram of the experimental setup.

Here U_i for $i = 1, 2$ denotes a unitary local transformation U_{U_i} of the form

$$U_{U_i} = \begin{pmatrix} \cos \vartheta_i & -\sin \vartheta_i \\ \sin \vartheta_i & \cos \vartheta_i \end{pmatrix} \begin{pmatrix} 1 & 0 \\ 0 & -1 \end{pmatrix} \begin{pmatrix} \cos \vartheta_i & \sin \vartheta_i \\ -\sin \vartheta_i & \cos \vartheta_i \end{pmatrix},$$

and γ denotes a non-unitary local transformation

$$A_\gamma = \begin{pmatrix} 1 & 0 \\ 0 & \gamma \end{pmatrix},$$

In Fig. 1, two of the qubits encounter non-unitary local transformations: qubit 1 is measured in some basis and post-selected, resulting in $\lambda_1^{\max} = 1$; qubit 4 is going through a filter operation given by A_γ . In the most general case, one can also apply local filter operations (or measurements) on the other qubits. However, a single filter (or measurement) may already suffice to ‘move around’ $\vec{\lambda}$ to non-overlapping regions of the polytopes, depending on the input state $|\Psi^{(i)}\rangle$.

Experimental setup – In our experiments, two different four-qubit states $|\Psi^{(1)}\rangle$ and $|\Psi^{(2)}\rangle$ are prepared, where

$$\begin{aligned} |\Psi^{(1)}\rangle &= \frac{\sqrt{3}}{3}(|HHHH\rangle + |VVVV\rangle) \\ &+ \frac{\sqrt{3}}{6}(|HV\rangle + |VH\rangle)(|HV\rangle + |VH\rangle), \quad (2) \end{aligned}$$

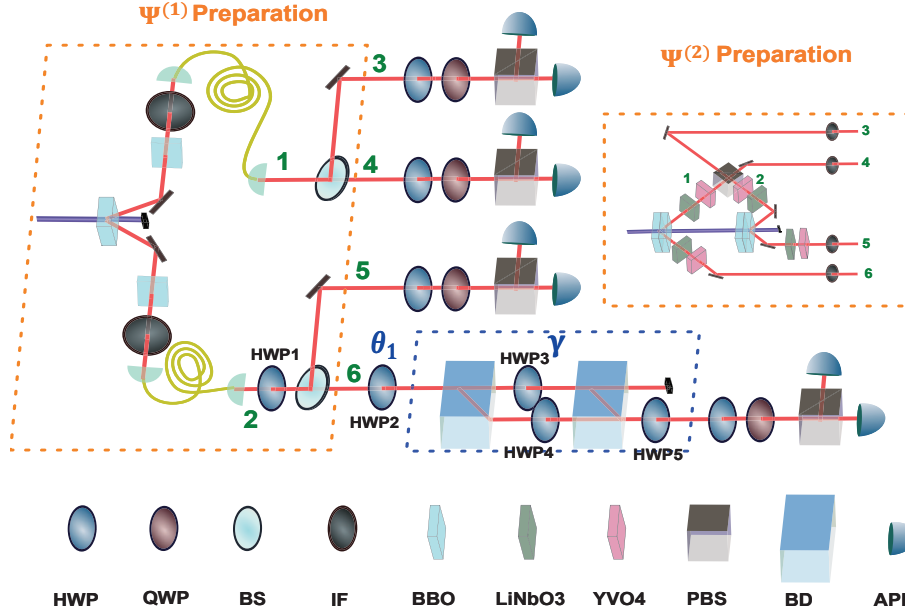


FIG. 2: Detailed configurations for preparing the states $\Psi^{(1)}$ and $\Psi^{(2)}$ and for realizing the operator A_γ are shown in the orange boxes and the blue box, where HWP3, HWP4 and HWP5 are rotated by $\frac{1}{2}(\arcsin \gamma)$, $\frac{\pi}{4}$, and $\frac{\pi}{4}$ respectively. The unitary operator U_{θ_1} is realized by HWP2 at specific angles. A QWP and a HWP in front of a polarization beam displacer (PBS) in each mode are used to implement the measurement in different bases for the standard state tomography. Post-selection in some basis of qubit 1 (the state of the photon in mode ‘3’) is realized by collecting only photons in one of the output modes of the PBS. The indices in the figure denote the spatial modes.

and $|\Psi^{(2)}\rangle$ is the four-qubit GHZ state

$$|\Psi^{(2)}\rangle = \frac{\sqrt{2}}{2}(|HHHH\rangle + |VVVV\rangle). \quad (3)$$

The qubits are encoded by horizontal $|H\rangle$ and vertical $|V\rangle$ polarization. The goal is to determine the entanglement type for each of the input state using the polytope method. For both $|\Psi^{(1)}\rangle$ and $|\Psi^{(2)}\rangle$, we have $\vec{\lambda} = (\frac{1}{2}, \frac{1}{2}, \frac{1}{2}, \frac{1}{2})$. That is, local spectra do not tell them apart, hence local filter operations are needed to ‘move around’ $\vec{\lambda}$.

The SLOCC orbit of the four-qubit GHZ state $|\Psi^{(2)}\rangle$ correspond to the full polytope $\mathcal{P}^{\text{full}}$. However, the state $|\Psi^{(1)}\rangle$ corresponds to a smaller polytope $\mathcal{P}^s \subset \mathcal{P}^{\text{full}}$ with vertices

$$\begin{aligned} &(\frac{1}{2}, \frac{1}{2}, \frac{1}{2}, \frac{1}{2}), (1, 1, 1, 1), \\ &(1, 1, \frac{1}{2}, \frac{1}{2}), (1, \frac{1}{2}, 1, \frac{1}{2}), (1, \frac{1}{2}, \frac{1}{2}, 1), \\ &(\frac{1}{2}, 1, 1, \frac{1}{2}), (\frac{1}{2}, 1, \frac{1}{2}, 1), (\frac{1}{2}, \frac{1}{2}, 1, 1). \end{aligned}$$

The smaller polytope \mathcal{P}^s is characterized by the additional constraint

$$f(\vec{\lambda}) = -\lambda_1^{\max} + \lambda_2^{\max} + \lambda_3^{\max} + \lambda_4^{\max} \geq 1 \quad (4)$$

and all permutations of it.

Our experimental setup for the states $|\Psi^{(1)}\rangle$ and $|\Psi^{(2)}\rangle$ is shown in Fig. 2. A 390 nm femto-second pump light,

frequency-doubled from a 780 nm mode-locked Ti:sapphire pulsed laser (with the pulse width about 150 fs and repetition rate 76 MHz) was used to pump the respective down-converter. For the preparation of $|\Psi^{(1)}\rangle$, a 2 mm type-II phase-matched BBO crystal is used as down-converter to produce two pairs of entangled photons [19], and two 1 mm BBO crystals are used to compensate the birefringence of *o*-light and *e*-light in the 2 mm BBO. HWP1 rotates the polarization of the photons in path ‘2’ (horizontal to vertical and vertical to horizontal). Then after the beam splitters (BS), the above two pairs of entangled photons are transformed into the state $|\Psi^{(1)}\rangle$. In mode ‘6’, we use two beam displacers and three half wave plates (HWPs, HWP3 is used for balancing the optical length of the two beams between partdisplacers) to construct the local filter A_γ . For the four-qubit GHZ state $|\Psi^{(2)}\rangle$ shown in the right part of Fig. 2, a cascaded sandwich beam-like BBO entangled source [20] is used. A PBS combines the photons from mode ‘1’ and ‘2’. We will get the four-qubit GHZ state $|\Psi^{(2)}\rangle$ if there is one photon in each of the modes ‘3’, ‘4’, ‘5’, and ‘6’ [21].

Results – We first perform full quantum state tomography to reconstruct the density matrix of $|\Psi^{(1)}\rangle$ and $|\Psi^{(2)}\rangle$, the fidelity of which are 0.9422 ± 0.0036 and 0.9001 ± 0.0038 . Then we collect data from each mode to obtain the corresponding single-qubit density matrix and calculate their local spectra for both states. As shown in Table I, the local spectra of $|\Psi^{(1)}\rangle$ and $|\Psi^{(2)}\rangle$ are almost identical, so we can not distinguish their entanglement polytopes.

To distinguish the entanglement polytopes of $|\Psi^{(1)}\rangle$ and

state	λ_1^{\max}	λ_2^{\max}	λ_3^{\max}	λ_4^{\max}	$f(\vec{\lambda})$
$ \Psi^{(1)}\rangle$	0.529(4)	0.514(4)	0.540(4)	0.530(4)	1.056(8)
$ \Psi^{(2)}\rangle$	0.521(4)	0.524(4)	0.535(4)	0.525(4)	1.062(8)

TABLE I: The local spectra λ_1^{\max} , λ_2^{\max} , λ_3^{\max} , λ_4^{\max} together with $f(\vec{\lambda})$ for the states $|\Psi^{(1)}\rangle$ and $|\Psi^{(2)}\rangle$. The uncertainties inside the brackets are obtained by Monte Carlo simulation (1000 steps).

	ϑ_1	γ	λ_2^{\max}	λ_3^{\max}	λ_4^{\max}	$f(\vec{\lambda})$
<i>a</i>	$\pi/8$	$1/\sqrt{2}$	0.609(10)	0.831(9)	0.701(10)	1.141(18)
<i>b</i>	$\pi/8$	$1/\sqrt{3}$	0.557(10)	0.850(9)	0.614(10)	1.021(17)
<i>c</i>	$\pi/8$	$1/\sqrt{5}$	0.603(10)	0.875(9)	0.553(10)	1.032(18)
<i>d</i>	$3\pi/32$	$1/\sqrt{5}$	0.713(9)	0.883(9)	0.717(8)	1.313(17)
<i>e</i>	0	1	0.657(9)	0.848(8)	0.857(8)	1.362(17)
<i>f</i>	0	1	0.525(9)	0.544(8)	0.516(8)	0.584(19)

TABLE II: Setting of the parameters ϑ_1 and γ for the data points labeled ‘*a* ~ *f*’, together with the measured local spectra λ_2^{\max} , λ_3^{\max} , λ_4^{\max} and the resulting value of $f(\vec{\lambda})$. The uncertainties inside the brackets are obtained by Monte Carlo simulation (1000 steps).

$|\Psi^{(2)}\rangle$, we then try to move $\vec{\lambda}$ out of the smaller polytope \mathcal{P}^s using local filters, as illustrated in Fig. 1. We fix $\vartheta_2 = -\pi/8$, and then measure the first qubit in the computational basis. By post-selection we have $\lambda_1^{\max} = 1$. For each setting of ϑ_1 and γ , we perform tomography of the qubits 2, 3, and 4 to determine the values of λ_2^{\max} , λ_3^{\max} , and λ_4^{\max} (see Table II). The smaller polytope \mathcal{P}^s is characterized by $f(\vec{\lambda}) \geq 1$.

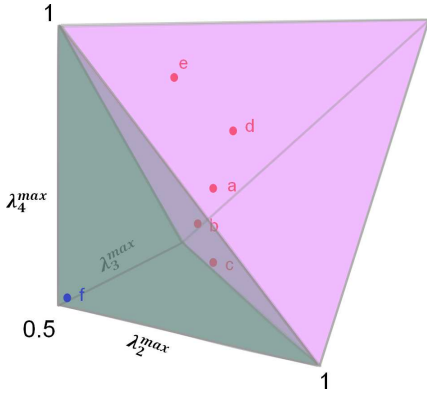


FIG. 3: Three-dimensional polytopes. The pink region and the blue region represent the polytope of $|\Psi^{(1)}\rangle$ and $|\Psi^{(2)}\rangle$ respectively. Experimental data ‘*a* ~ *e*’ is for $|\Psi^{(1)}\rangle$ while ‘*f*’ is for $|\Psi^{(2)}\rangle$. Error bars are too small to identify (see Table II).

The results are illustrated in Fig. 3 and 4. In Fig. 3, the data is shown in the three-dimensional polytope for λ_2^{\max} , λ_3^{\max} , λ_4^{\max} as by post-selection of the first qubit, $\lambda_1^{\max} = 1$. The smaller polytope \mathcal{P}^s be-

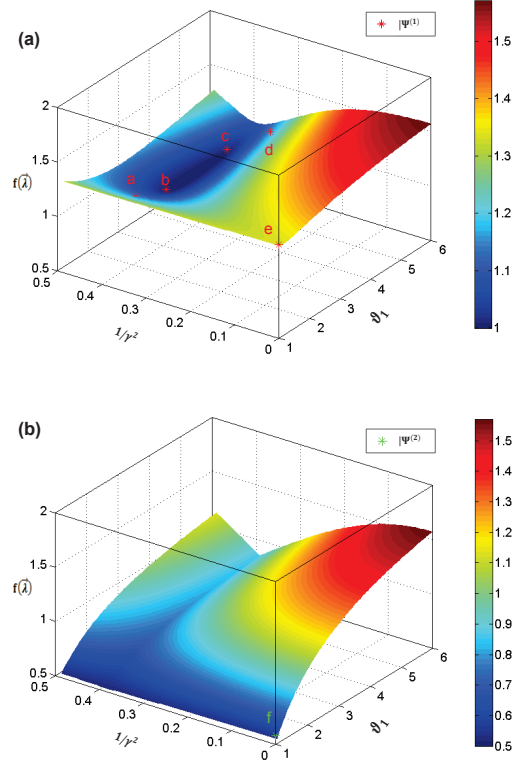


FIG. 4: Experimental and theoretical results for $f(\vec{\lambda})$ as a function of ϑ_1 and $1/\gamma^2$. (a) shows the plot for the state $|\Psi^{(1)}\rangle$ together with the experimental data points ‘*a* ~ *e*’. (b) shows the plot for the state $|\Psi^{(2)}\rangle$ and the data point ‘*f*’ from the experiment. Error bars are too small to identify (see Table II).

comes a three-dimensional polytope $\tilde{\mathcal{P}}^s$ with vertices $(1, 1/2, 1/2)$, $(1/2, 1, 1/2)$, $(1/2, 1/2, 1)$, $(1, 1, 1)$, and the full polytope $\mathcal{P}^{\text{full}}$ becomes a three-dimensional polytope $\tilde{\mathcal{P}}^{\text{full}}$ which contains $\tilde{\mathcal{P}}^s$ and has an additional vertex $(1/2, 1/2, 1/2)$. The data point *f* of the state $|\Psi^{(2)}\rangle$ outside of $\tilde{\mathcal{P}}^s$ shows that $|\Psi^{(2)}\rangle$ is not in \mathcal{P}^s . In contrast, the data points *a, b, c, d, e* obtained from $|\Psi^{(1)}\rangle$ all lie in $\tilde{\mathcal{P}}^s$, which indicates that $|\Psi^{(1)}\rangle$ belongs to \mathcal{P}^s . This shows that $|\Psi^{(1)}\rangle$ and $|\Psi^{(2)}\rangle$ have different entanglement types.

In Fig 4, the plot of $f(\vec{\lambda})$ as a function of ϑ_1 and $1/\gamma^2$ is shown. For the smaller polytope \mathcal{P}^s , the inequality $f(\vec{\lambda}) \geq 1$ always holds. A violation of this inequality signals that the state $|\Psi^{(2)}\rangle$ (point *f*) is not in \mathcal{P}^s . In contrast, the data points *a, b, c, d, e* obtained for $|\Psi^{(1)}\rangle$ all satisfy $f(\vec{\lambda}) \geq 1$, which indicates that $|\Psi^{(1)}\rangle$ belongs to \mathcal{P}^s . This shows that $|\Psi^{(1)}\rangle$ and $|\Psi^{(2)}\rangle$ have different entanglement types.

Since the first photon of the four-qubit state is post-selected and the last photon goes through a non-unitary filter, the probability of success for the experiment is 0.2917, 0.2222, 0.1667, 0.1768, 0.5, and 0.5 for our experimental data ‘*a* ~ *f*,’ respectively.

Because the birefringence of the *o*-light and the *e*-light

in the BBO (down-converter) cannot be compensated completely, and because of the high-term noise from the SPDC process and some mode mismatch, we do not obtain the pure states $|\Psi^{(1)}\rangle$ and $|\Psi^{(2)}\rangle$, but some noisy version of them. Nonetheless, the errors in our experiment are mainly due to the time uncertainty of the photon pairs generated in the BBO. The coincidence counts obey a Poisson distribution, the parameters of which we estimate from the experimental data. Then we perform Monte Carlo simulation to estimate the errors indicated in Tables I and II.

Summary – We experimentally demonstrate the detection of entanglement polytopes in a four-qubit system. We use local filters to effectively distinguish states with the same single-particle spectra, but which belong to different polytopes. This provides a new tool to experimental detection of entanglement in a multi-qubit system using only local operations.

Acknowledgements – The work in USTC is supported by National Fundamental Research Program (Grants No. 2011CBA00200 and No. 2011CB9211200), National Natural Science Foundation of China (Grants No. 61108009 and No. 61222504). B.Z. is supported by NSERC and CIFAR.

* Electronic address: gyxiang@ustc.edu.cn

- [1] R. Horodecki, P. Horodecki, M. Horodecki, and K. Horodecki, *Reviews of Modern Physics* **81**, 865 (2009).
- [2] A. Acin, A. Andrianov, E. Jane, and R. Tarrach, *Journal of Physics A: Mathematical and General* **34**, 6725 (2001).
- [3] L. Chen, D. Z. Dokovic, M. Grassl, and B. Zeng, *Journal of Mathematical Physics* **55**, 082203 (2014).
- [4] L. Chen, J. Chen, D. Z. Dokovic, and B. Zeng, *Communications in Mathematical Physics* **333**, 541 (2015).
- [5] W. Dür, G. Vidal, and J. I. Cirac, *Physical Review A* **62**, 062314 (2000).
- [6] F. Verstraete, J. Dehaene, B. De Moor, and H. Verschelde, *Physical Review A* **65**, 052112 (2002).
- [7] O. Chterental and D. Z. Dokovic, *Linear Algebra Research Advances*, G. D. Ling (Ed.) pp. 133–167 (2007).
- [8] V. Coffman, J. Kundu, and W. K. Wootters, *Physical Review A* **61**, 052306 (2000).
- [9] O. Gühne and G. Tóth, *Physics Reports* **474**, 1 (2009).
- [10] M. Walter, B. Doran, D. Gross, and M. Christandl, *Science* **340**, 1205 (2013).
- [11] A. Sawicki, M. Oszmaniec, and M. Kus, *Physical Review A* **86**, 040304 (2012).
- [12] A. Sawicki, M. Oszmaniec, and M. Kus, *Reviews in Mathematical Physics* **26** (2014).
- [13] G. Aguilar, S. Walborn, P. Ribeiro, and L. Céleri, Preprint arXiv:1412.2401 (2014).
- [14] F. Verstraete, J. Dehaene, and B. DeMoor, *Physical Review A* **64**, 010101 (2001).
- [15] Z.-W. Wang, X.-F. Zhou, Y.-F. Huang, Y.-S. Zhang, X.-F. Ren, and G.-C. Guo, *Physical Review Letters* **96**, 220505 (2006).
- [16] Y.-K. Bai and Z. Wang, *Physical Review A* **77**, 032313 (2008).
- [17] S. Campbell, M. Tame, and M. Paternostro, *New Journal of Physics* **11**, 073039 (2009).
- [18] T. Bastin, C. Thiel, J. von Zanthier, L. Lamata, E. Solano, and G. Agarwal, *Physical Review Letters* **102**, 053601 (2009).
- [19] P. G. Kwiat, K. Mattle, H. Weinfurter, A. Zeilinger, A. V. Sergienko, and Y. Shih, *Physical Review Letters* **75**, 4337 (1995).
- [20] C. Zhang and et al, in preparation (2015).
- [21] J.-W. Pan, D. Bouwmeester, M. Daniell, H. Weinfurter, and A. Zeilinger, *Nature* **403**, 515 (2000).
- [22] W. Dür, G. Vidal, and J. I. Cirac, *Physical Review A* **62**, 062314 (2000), arXiv:quant-ph/0005115.
- [23] F. Verstraete, J. Dehaene, B. De Moor, and H. Verschelde, *Physical Review A* **65**, 052112 (2002), arXiv:quant-ph/0109033.
- [24] O. Chterental and D. Ž. Đoković, in *Linear Algebra Research Advances*, edited by G. D. Ling (Nova Science Publishers, 2007), chap. 4, pp. 133–167.
- [25] L. Lamata, J. León, D. Salgado, and E. Solano, *Physical Review A* **75**, 022318 (2007), arXiv:quant-ph/0610233.
- [26] D. Li, X. Li, H. Huang, and X. Li, *Quantum Information & Computation* **9**, 778 (2009), arXiv:0712.1876 [quant-ph].
- [27] J.-G. Luque and J.-Y. Thibon, *Physical Review A* **67**, 042303 (2003), arXiv:quant-ph/0212069.
- [28] E. Briand, J.-G. Luque, and J.-Y. Thibon, *Journal of Physics A: Mathematical and General* **36**, 9915 (2003), arXiv:quant-ph/0304026.
- [29] M. Walter, B. Doran, D. Gross, and M. Christandl, *Science* **340**, 1205 (2013), arXiv:1208.0365 [quant-ph].
- [30] A. Sawicki, M. Oszmaniec, and M. Kuś, *Reviews in Mathematical Physics* **26**, 1450004 (2014), arXiv:1208.0556 [math-ph].
- [31] M. Christandl, B. Doran, S. Kousidi, and M. Walter, *Communications in Mathematical Physics* **332**, 1 (2014), arXiv:1204.0741 [quant-ph].

APPENDIX

A. Entanglement polytopes

Two quantum states $|\psi_1\rangle$ and $|\psi_2\rangle$ are said to be equivalent with respect to SLOCC if there exists a sequence of local operations and classical communication that converts the state $|\psi_1\rangle$ into $|\psi_2\rangle$ with non-zero probability $p_{1\rightarrow 2} > 0$, and another protocol for the conversion of $|\psi_2\rangle$ into $|\psi_1\rangle$ that succeeds with probability $p_{2\rightarrow 1} > 0$. As we only require the success probabilities to be non-zero, it is sufficient to consider one branch of the protocol that has non-zero success probability. Thus we can, for example, write

$$\sqrt{p_{1\rightarrow 2}}|\psi_2\rangle = M_1 \otimes M_2 \otimes \cdots \otimes M_n |\psi_1\rangle, \quad (5)$$

where the matrices M_i correspond to the combination of all operations performed on particle i . In [22] it was shown that the matrices M_i in (5) can be replaced by invertible matrices. Moreover, all matrices can be chosen to have determinant one, combining all scalar factors with the success probability. Hence we have that the states $|\psi_1\rangle$ and $|\psi_2\rangle$ are in the same SLOCC class if and only if there is a non-zero constant $\lambda \in \mathbb{C}$ and matrices $A_i \in \text{SL}(d_i)$ (where d_i denotes the dimension of subsystem i) such that

$$\lambda |\psi_2\rangle = A_1 \otimes A_2 \otimes \cdots \otimes A_n |\psi_1\rangle. \quad (6)$$

Results on the classification of pure four-qubit states with respect to SLOCC can be found in [23–26]. Note that in the literature, sometimes the scaling factor λ is incorrectly ignored.

Unlikely the situation for local unitary transformations, polynomial invariants of the group $\text{SL}(d)^{\otimes n}$ yield only a necessary condition for SLOCC equivalence of two quantum states.

Proposition 1 *Let f_1, \dots, f_m be homogeneous polynomial invariants of the group $\text{SL}(d)^{\otimes n}$. If the normalized states $|\psi_1\rangle$ and $|\psi_2\rangle$ are in the same SLOCC class, then there exists a non-zero constant $\lambda \in \mathbb{C}$ such that*

$$f_i(|\psi_1\rangle) = f_i(\lambda |\psi_2\rangle) = \lambda^{\deg f_i} (|\psi_2\rangle) \quad \text{for } i = 1, \dots, m. \quad (7)$$

In the case of four qubits, we have four polynomial invariants B_{0000} , $D_{0000}^{(1)}$, $D_{0000}^{(2)}$, and F_{0000} of degree 2, 4, 4, and 6, respectively, see [27].

In order to get a necessary and sufficient criterion to decide SLOCC equivalence, one may consider covariants. Two vectors are in the same orbit of the group $\text{SL}(d)^{\otimes n}$ if and only if all covariants agree. Again, one has to take care of the scaling parameter λ to apply this criterion. In the case of four qubits, there are 170 covariants, see [28].

It has been shown that the points corresponding to the (sorted) spectra of the single-particle reduced density matrices of pure quantum states in the closure of an orbit under SLOCC transformations form a so-called *entanglement polytope*, see [29, 30]. The vertices of the polytope correspond to the covariants that do not vanish.

B. Four-qubit Polytopes

In the case of four qubits, there are 7 different 4-dimensional polytopes up to permutation of the qubits [29]. Lower-dimensional polytopes correspond to states that partially factorize. When we also consider the permutations, the polytopes \mathcal{P}_3 and \mathcal{P}_6 come in 6 different versions, while the polytopes \mathcal{P}_1 and \mathcal{P}_2 split into 4 different subtypes. The vertices of all polytopes are listed in Table III. The polytope \mathcal{P}_5 is contained in all other polytopes, and the polytope $\mathcal{P}_7 = \mathcal{P}^{\text{full}}$ is the largest polytope containing all states. Fig. 5 illustrates how the polytopes are contained in each other.

In the experiment, we investigate the four-qubit state

$$|\Psi^{(1)}\rangle = \frac{\sqrt{3}}{3}(|HHHH\rangle + |VVVV\rangle) + \frac{\sqrt{3}}{6}(|HV\rangle + |VH\rangle)(|HV\rangle + |VH\rangle), \quad (8)$$

and the four-qubit GHZ state

$$|\Psi^{(2)}\rangle = \frac{\sqrt{2}}{2}(|HHHH\rangle + |VVVV\rangle). \quad (9)$$

The qubits are encoded by horizontal $|H\rangle$ and vertical $|V\rangle$ polarization. Evaluating the covariants from [28] for the states $|\Psi^{(1)}\rangle$ and $|\Psi^{(2)}\rangle$ we find that the corresponding polytopes are $\mathcal{P}^s = \mathcal{P}_4$ and the full polytope $\mathcal{P}^{\text{full}} = \mathcal{P}_7$, respectively. The polytope \mathcal{P}_4 is obtained from \mathcal{P}_7 by removing the vertex $(1/2, 1/2, 1/2, 1)$ and all its permutations. The discriminating inequalities are

$$f(\vec{\lambda}) = -\lambda_1^{\max} + \lambda_2^{\max} + \lambda_3^{\max} + \lambda_4^{\max} \geq 1 \quad (10)$$

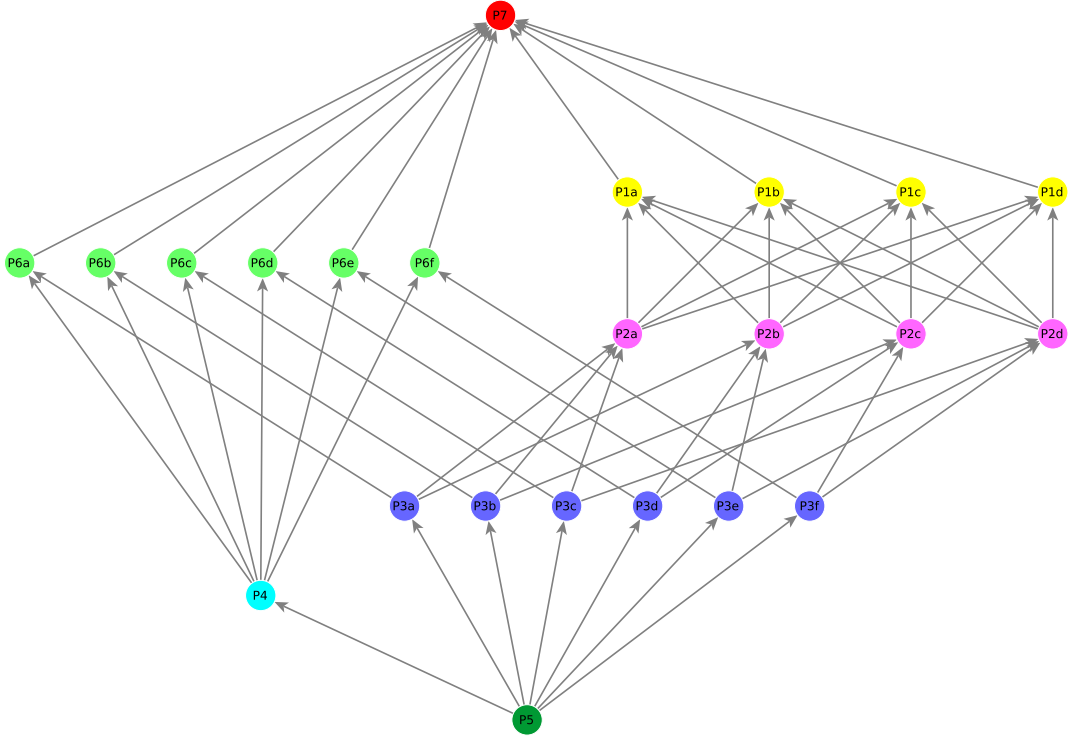


FIG. 5: Lattice of the different entanglement polytopes for four qubits. Note that, in general, the polytopes intersect non-trivially.

and all its permutations.

C. Volume of the Polytopes

In the case of three qubits, we have only two three-dimensional polytopes $\mathcal{P}^W \subset \mathcal{P}^{GHZ}$ corresponding to the SLOCC class containing the W -state and the GHZ -state, respectively. Picking a pure three-qubit state with respect to the Haar measure at random, the resulting distribution of the eigenvalues of the local density matrices has been computed in [31]. From this one finds that the volume of the sub-polytope \mathcal{P}^W is $203/216 \approx 93.98\%$. Hence the probability for a random three-qubit state to have a local spectra corresponding to a point outside the polytope \mathcal{P}^W is only $13/216 \approx 6.02\%$.

For four qubits, we computed the local spectra of 10^6 random pure states and determined which of the polytopes contains the vector of local spectra. The results are summarized in Table IV. While the polytope \mathcal{P}_4 corresponding to the state $|\Psi^{(1)}\rangle$ of our experiment is fairly low in the hierarchy of polytopes (see Fig. 5), the local spectra of only 9522 out of one million random states violate the discriminating inequalities (10). Hence, the chance for a random four-qubit state to have a local spectrum that lies outside of \mathcal{P}_4 is only about 0.95%. This clearly indicates that one has to apply local filters in order to get information about the entanglement polytopes.

Note that after measuring one of the qubits and post-selection of the measurement outcome, we have a four-qubit state that factors into a single qubit and a three-qubit state. The polytope \mathcal{P}_4 is mapped to the three-qubit polytope \mathcal{P}^W which has a volume of about 94%. Hence the local measurement increases the chance for a random state to lie outside the smaller polytope from less than one percent to about six percent.

[illegible]

TABLE III: The different entanglement polytopes for four qubits given by their vertices

\mathcal{P}_1 996 761	\mathcal{P}_1^a 990 140	\mathcal{P}_1^b 990 137	\mathcal{P}_1^c 990 204	\mathcal{P}_1^d 990 262		
\mathcal{P}_2 863 481	\mathcal{P}_2^a 705 172	\mathcal{P}_2^b 704 928	\mathcal{P}_2^c 704 932	\mathcal{P}_2^d 704 791		
\mathcal{P}_3 781 562	\mathcal{P}_3^a 607 121	\mathcal{P}_3^b 607 010	\mathcal{P}_3^c 607 176	\mathcal{P}_3^d 606 791	\mathcal{P}_3^e 606 925	\mathcal{P}_3^f 607 051
\mathcal{P}_4 990 478	\mathcal{P}_4 990 478					
\mathcal{P}_5 130 165	\mathcal{P}_5 130 165					
\mathcal{P}_6 1 000 000	\mathcal{P}_6^a 995 287	\mathcal{P}_6^b 995 277	\mathcal{P}_6^c 995 320	\mathcal{P}_6^d 995 158	\mathcal{P}_6^e 995 201	\mathcal{P}_6^f 995 191
\mathcal{P}_7 1 000 000	\mathcal{P}_7 1 000 000					

TABLE IV: Distribution of 1 000 000 random pure states on the different entanglement polytopes. In the first column we list the union of the different permuted polytopes of the same type.